

An improved paradigm for modeling animal flights at moderate Reynolds numbers

Kyohei Onoue^{*†}

Hamid Vejdani^{*†}

Yunxing Su^{*}

Kenneth S. Breuer^{*‡}

^{*}Fluids and Thermal Sciences, School of Engineering, Brown University, Providence, RI 02912, USA.

[†]Kyohei Onoue and Hamid Vejdani contributed equally to the present work

[‡]Author for correspondence (email: kenneth_breuer@brown.edu)

Abstract

We report on experimental and numerical studies aimed at developing an improved paradigm for modeling avian flights at moderate Reynolds numbers. A series of experiments were performed to characterize the behaviors of aerodynamic forces and moment associated with a quasi-steady rectangular wing over a range of incidence angles, α . We demonstrate that, while the drag coefficient curve, $C_D(\alpha)$, can be accurately modeled solely by a simple trigonometric function, the evolution of lift coefficient curve, $C_L(\alpha)$, is governed by the sum of trigonometric and exponential functions, where the latter captures the linear variation in lift coefficient within the small-angle regime, as predicted by the linear inviscid theory. In addition, we establish an empirical relation between the location of the center of pressure and the incidence angle, which can be used in conjunction with the proposed aerodynamic formulas (i.e. C_L and C_D) to evaluate the pitching moment coefficient, $C_M(\alpha)$, about any arbitrary axis. These quasi-steady formulations are then utilized to simulate forward flight of a model that possesses dynamical characteristics of a pigeon across various flight speeds, and the results are compared against previously-reported experimental data on pigeons. We successfully demonstrate that the proposed formulas yield accurate predictions of the wing-beat frequency, at least over a range of Reynolds numbers spanning from approximately 70,000 to 150,000.

Introduction

There has been a substantial interest in understanding the physics behind birds and bats flapping flight, both to understand the mechanics of these natural fliers and also to develop Micro Air Vehicles (MAVs) with similar physics and size range. The majority of research so far has been done on relatively small fliers like insects with Reynolds numbers less than 1000 (e.g. Dickinson and Götze, 1993; Dickinson et al., 1999; Sane and Dickinson, 2001, 2002; Berman and Wang, 2007), while for bigger fliers like birds and bats the Reynolds number

would increase to around 40,000. In addition, the vast majority of current Micro Air Vehicles (MAVs) operate at this medium range Reynolds numbers and for designing controllers and studying the stability for these vehicles a computationally-efficient aerodynamic modeling is required.

The wing aerodynamic model proposed by Dickinson et al. (1999); Sane and Dickinson (2001, 2002) has been extensively used for modeling aerodynamic forces (e.g., see, Parslew and Crowther, 2010; Parslew, 2014; Cheng et al., 2016; Chin and Lentink, 2016) due to its simple nature and low computational cost, which makes it useful for dynamical modeling, control and optimization calculations. In Parslew and Crowther (2010) and Parslew (2014), pigeon size models were analyzed for different flight modes (cruise, climbing and descending) over a range of forward speeds. Cheng et al. (2016) employed the quasi-steady modeling for analyzing the mechanics of scape maneuvers in hummingbirds using the same format for translational lift and drag but with values adjusted for hummingbirds.

Although the quasi-steady formulation of Dickinson et al. (1999) has been developed specifically for insects with small Reynolds numbers, it has also been used for larger Reynolds numbers (Byl, 2010; Chen et al., 2010; Parslew and Crowther, 2010; Parslew, 2014; Stowers and Lentink, 2015; Cheng et al., 2016; Read et al., 2016). While for low Reynolds numbers and insect wings the augmented lift and drag from the stabilized leading-edge vortex (LEV) can be useful, the increased drag can be seriously deteriorating for large Reynolds numbers in forward speeds. We intend in this study to propose improvements in calculating the aerodynamic forces in the quasi-steady formulation for moderate Reynolds numbers pertinent to avian flights.

Materials and methods

All experiments were conducted in a closed-return water channel with a test section of 0.8 m in width and 0.6 m in depth. Fig 1A illustrates a flat plate, with chord, $c = 0.076$ m, span,

$h = 0.456$ m and thickness, $\delta = 8$ mm, rigidly affixed to the 6-axis force transducer (Delta IP65, ATI Industrial Automation), in a uniform free-stream with velocity, U , and density, ρ_f . The free-stream velocity was monitored in real time using an acoustic doppler velocimeter (Vectrino, Nortek AS). The force transducer measures the normal, F_N , and tangential, F_T , forces, as well as the pitching moment, M , about the rotational axis located at the mid-chord point; these forces are related to lift, L , and drag, D , through the geometry shown in Fig 1B, i.e. $L = F_N \cos(\alpha) - F_T \sin(\alpha)$ and $D = F_N \sin(\alpha) + F_T \cos(\alpha)$, where α denotes the geometric angle of attack. The angle of attack is modulated by sending an open-loop command to the rotary stepper motor (Nema23 D600, Applied Motion Products) and the corresponding value is measured via an optical encoder (E3 optical encoder, US Digital). In this study, the Reynolds number, based on the chord length, is defined as $Re = Uc/\nu$, where ν denotes the kinematic viscosity of the fluid. Given that the chord length represents less than 10% of the test section width, the blockage and side-wall boundary layer effects were deemed minor. Due to the use of a large aspect ratio ($AR = 6$) rectangular plate, the flow associated with the present study is expected to be largely two-dimensional, and the validity of this assumption will be justified in the subsequent section.

In the present investigation, the steady-state forces and moment associated with a steady flat plate immersed in a uniform flow were measured over a broad range of angles of attack ($\alpha = 0^\circ \sim 110^\circ$, $\Delta\alpha = 2^\circ$) at four different Reynolds numbers varying from 20,000 to 50,000 at an increment of 10,000. At each angle of attack, the measurements were recorded for 30 seconds, but only the last 20 seconds of the recording was analyzed during the post-processing in order to isolate the transient response. The reproducibility of the results was confirmed by repeating the same set of experiments three times.

Results and discussion

0.1 Part I: quasi-steady aerodynamic formulations

The evolutions of lift and drag coefficient curves as a function of the angle of attack are illustrated in Figs. 2A and B, respectively, where $C_L = 2L/\rho_f U^2 ch$ and $C_D = 2D/\rho_f U^2 ch$. The lift and drag coefficients are well approximated by the following empirical relationships in terms of α (in degrees):

$$\begin{aligned} C_L(\alpha) &= -0.44e^{-0.47\alpha} + 1.19\sin(1.74\alpha + 20^\circ) \\ C_D(\alpha) &= 1.04 + \sin(1.72\alpha - 70^\circ), \end{aligned} \tag{1}$$

where, in each case, the best-fit regression curve with a 95% confidence interval yielded an R-squared value greater than 0.995. As illustrated in Fig. 2A, the C_L curve follows closely the steady thin airfoil theory prediction with a slope of $dC_L/d\alpha = 2\pi$ at small angles of attack ($\alpha < 8^\circ$). One can infer that the laminar boundary layer separation occurs at approximately $\alpha \approx 8^\circ$, and that the apparent lift augmentation at large angles of attack is presumably due to: (1) the large-scale steady separation from the sharp leading and trailing edges, (2) the pressure accumulation on the frontal surface and (3) the viscous stress induced by the uniform flow. It should be noted that the forces measured in the present study are “quasi-steady” such that the concomitant shedding of von Kármán vortices behind the plate does not induce any measurable time-dependency in the forces and the pitching moment imparted on the wing. This is presumably because the formation of these large-scale vortices occurs in the far-wake region approximately 1.5 to 2 chord lengths downstream of the plate (for Reynolds numbers on the order of $\mathcal{O}(10^4) \sim \mathcal{O}(10^5)$), as discussed in Onoue and Breuer (2016) and Liu et al. (2017). The validity of the present assertion is also supported by small standard deviations associated with the force and moment data presented in Fig. 2, reflecting minor unsteadiness in the measurements. While the present observation is in contrast to the reports

of Dickinson and Götz (1993) and Wang (2000), where the generation of a von Kármán street resulted in an oscillatory behavior in the force curves at post-stall angles, one can attribute this discrepancy to differences in the Reynolds numbers. Upon the attainment of maximum lift coefficient at approximately $\alpha \approx 40^\circ$, the lift curve decays monotonically as α is further increased.

As shown in Fig. 2B, the drag coefficient increases monotonically from approximately 0.1 at $\alpha = 0$ to a maximum value of 2.0 at $\alpha \approx 90^\circ$, conforming very well with the theoretical prediction of 1.95, wherein the drag coefficient associated with a 2D flat plate facing perpendicular to the incoming flow can be approximated as $C_D = 1.95 + 50/Re$ (Ellington, 1991). In addition, the magnitudes of C_L and C_D are comparable to similar steady-state measurements made on a translating 2D rectangular wing at various fixed angles of attack (Dickinson and Götz, 1993). A good agreement with the aforementioned studies justifies our previous statement that the flat plate employed in the current study can, in fact, be treated as nominally 2D. Interestingly, the drag coefficient curve at high Reynolds numbers can be well approximated with a simple harmonic relationship that closely resembles the form derived in the experimental work of Dickinson et al. (1999), where the authors reported on the steady-state translational forces (i.e. C_L and C_D) on a dynamically scaled-up *Drosophila* wing undergoing a 180° constant velocity rotation at fixed angles of attack at a Reynolds number of approximately 140. With the exception of this similarity, however, the general characteristics of the present force profiles differ conspicuously from those of Dickinson et al. (1999). First we note that, while our C_L values conform with the thin airfoil theory predictions for small angles, Dickinson et al. (1999) largely underestimates the theoretical prediction of $dC_L/d\alpha = 2\pi$ with a value of approximately 3.8. This discrepancy is attributable to the violation of the inviscid flow assumption—the basis of the thin airfoil theory (Bisplinghoff et al., 1957)—in the study of Dickinson et al. (1999), where the experiments were conducted at a low Reynolds number of $\mathcal{O}(10^2)$ using the mineral oil as the working fluid medium. Secondly, the maximum C_L and C_D obtained in the present study are approximately 45% and 65%

smaller, respectively. Higher steady-state aerodynamic forces associated with a rotating 3D wing is due, in part, to the formation, growth and subsequent stabilization of an “attached” leading-edge vortex (LEV) on the upper surface of the wing during its unsteady motion, as previously noted by a number of investigators (e.g. Maxworthy, 1981; Ellington et al., 1996; Dickinson et al., 1999). The general consensus in the archival literature is that the parameter of rotation (e.g. revolving, flapping and pitching) plays an important role in the formation and subsequent stabilization of the LEV (e.g. Lentink and Dickinson, 2009; Wong and Rival, 2015; Onoue and Breuer, 2016), and that this enhanced vortex stability is directly correlated to the generation of strong aerodynamic forces (Granlund et al., 2013; Harbig et al., 2013) and pitching moments (Onoue et al., 2015; Onoue and Breuer, 2016) that far exceed their static counterparts, easily by a factor of 1.5 to 2.5 in magnitude.

Another useful contribution of the present study is the establishment of a simple empirical relation between the location of the center of pressure and the angle of attack. We determined the chordwise location of the center of pressure (measured from the leading edge) using the formula: $x_{cp}^* = 0.5 - M/F_N c$. Fig 2D illustrates the evolution of x_{cp}^* as a function of α at four distinct Reynolds numbers, where all four cases collapse nicely. An empirical fit of x_{cp}^* is given by Eqn 2, from which one can evidently infer that the current model predicts that x_{cp}^* approaches the aerodynamic center at 0.25 in the limit as α tends to zero, which resonates well with the linear inviscid theories (e.g. Wagner, 1925; Theodorsen, 1935; Garrick, 1936).

$$x_{cp}^*(\alpha) = 0.247 + 0.016\alpha^{0.6} + 0.026\alpha e^{-0.11\alpha}. \quad (2)$$

It should be mentioned that the moment coefficient, $C_M = C_N(x^* - x_{cp}^*)$, about any arbitrary point can be easily approximated using Eqns 1 and 2, where the normal force coefficient is defined as $C_N = C_L \cos(\alpha) + C_D \sin(\alpha)$ and x^* denotes the location of the moment axis with respect to the leading edge (e.g. $x^* = 0.25$ for the quarter-chord point). Using this formulation, we evaluated the moment coefficient about the mid-chord point ($x^* = 0.5$),

and the result is plotted in Fig 2C with a yellow curve, revealing an excellent agreement with the experimental measurements (plotted with open circles); note that the empirical data are normalized as $C_M = 2M/\rho_f U^2 c^2 h$. Finally, it is worthwhile mentioning that the differentiable nature of the proposed formulas makes them suitable to be used in dynamical simulations that utilize gradient-based optimization techniques to determine, for example, power-optimal kinematics of avian wings for different modes of flight.

0.2 Part II: simulation

In order to validate the efficacy of the proposed formulas in modeling avian flights at moderate Reynolds numbers, we simulated forward flight of a model that replicates dynamical characteristics of a pigeon across various cruise velocities. The model has two translational degrees of freedom ($x - z$) and one rotational degree of freedom in pitch (ψ), where the latter accounts for the changes in the body angle, as illustrated in Fig 3A. One of the salient characteristics of the flight of a pigeon is that the body angle, as well as the wing's incidence angle, appear to be a function of the cruise velocity, which can be appropriately modeled by the pitch degree of freedom, see, e.g., Tobalske et al. (2003) and Parslew (2014). In addition to generating flapping and pronation/supination motions, the model is allowed to modulate its wingspan during the wingbeat cycle in order to replicate basic wing kinematics of a pigeon. For aerodynamic modeling, we employed a blade element model and evaluated the forces exerted on each blade element using the proposed formulations (Eqns 1 and 2) and those of Dickinson et al. (1999). The morphometric characteristics and the wing kinematics of the pigeon are assumed from Tobalske and Dial (1996) with the whole mass $M = 0.316$ kg, length of each wing $l_0 = 27.9$ cm and average wing chord $c = 11.2$ cm.

Fig 3B compares the predicted wingbeat frequency associated with the steady-state forward flight using the proposed formulas and those established by Dickinson et al. (1999). The results from these simulations are then compared against the experimental measurements on pigeons by Tobalske and Dial (1996). For high forward velocities ($U > 10$ m/s),

our formulas perform remarkably well in predicting the actual wingbeat frequencies, while the formulations of Dickinson et al. (1999) result in a poor agreement with the empirical observations. This discrepancy is presumably due to large drag, which can only be compensated by generating sufficient thrust via an increase in the wingbeat frequency; note that the incidence angle of the pigeon wing was previously measured by Hedrick et al. (2002), and estimated to be less than 15° at high cruise speeds ($U > 9$ m/s). As the forward velocity decreases, the importance of cruise velocity becomes less pronounced, and the model tries to generate sufficient lift by either increasing the wingbeat frequency, modulating the angle of attack (α) to a larger value or both; recall that ψ and α increase as the cruise speed is decreased (see Parslew (2014)). Therefore, if the maximum lift coefficient is insufficient, the model must inevitably increase the wingbeat frequency to balance out this deficiency. Therefore, the fact that our formulation overestimates the actual wingbeat frequency, which remains nearly constant over a range of forward velocities as depicted in Fig 3B, suggests that the peak lift coefficient provided by our formula is inadequate. Furthermore, it is interesting to note that the predicted wingbeat frequency (based on the formulation of Dickinson et al. (1999)) appears to converge monotonically to the measurement of Tobalske and Dial (1996) as the forward velocity decreases; this observation may point to the importance of rotational movement of the wing in elevating the performance gains in aerodynamic forces, in particular at lower flight velocities where the body angle (ψ), as well as the wing's incidence angle (α), are conspicuously large (see, e.g, Fig 5 of Parslew, 2014). The current assertion is also in line with the fact that the rotational excursion of the wing is pronounced during hovering, which presumably helps improve the wing's overall aerodynamic performance at post-stall angles by promoting the stability, and thus the attachment, of the LEV over the suction side of the wing, as noted previously. In essence, we hypothesize that the overprediction of the wingbeat frequency at lower flight velocities is a manifestation of the fact that a purely translating wing (as in the current geometry) cannot leverage the dynamic-stall process (owing to lack of rotational maneuver that stabilizes and prolongs the vortex attachment) and that

the von Kármán vortices associated with the present measurements are fully detached from the lifting surface (presumably due to small convective time scales associated with Reynolds numbers on the order of $\mathcal{O}(10^4)$), both of which lead to notably smaller steady-state force coefficients (for large α) relative to those reported by Dickinson et al. (1999) for a revolving *Drosophila* wing at a Reynolds number on the order of $\mathcal{O}(10^2)$.

Acknowledgements

The authors would like to thank the members of the Energy Harvesting group at Brown University for their contributions to the development of the experimental apparatus.

Competing interests

The authors declare no competing financial interests.

Author contributions

K.O and H.V. drafted the paper; K.O., H.V. and Y.S. designed and executed the experiments; K.O. characterized the aerodynamic models; H.V. performed numerical simulations.

Funding

This research is supported by the Department of Energy's Advanced Research Projects Agency-Energy (ARPA-E).

References

- Berman, G. J. and Wang, Z. J.** (2007). Energy-minimizing kinematics in hovering insect flight. *J. Fluid Mech.* **582**, 153–168.
- Bisplinghoff, R. L., Ashley, H. and Halfman, R. L.** (1957). *Aeroelasticity*. Cambridge, Massachusetts: Addison-Wesley Publishing Co. Inc.
- Byl, K.** (2010). A passive dynamic approach for flapping-wing micro-aerial vehicle control. In *ASME 2010 Dynamic Systems and Control Conference*, pp. 215–223.
- Chen, L., Guan, Y., Zhang, X. and Zhang, H.** (2010). Improvement of an aerodynamic model for biomimetic flapping-wing robots. In *2010 IEEE/ASME International Conference on Advanced Intelligent Mechatronics*, pp. 49–54.
- Cheng, B., Tobalske, B. W., Powers, D. R., Hedrick, T. L., Wang, Y., Wethington, S. M., Chiu, G. T.-C. and Deng, X.** (2016). Flight mechanics and control of escape manoeuvres in hummingbirds ii. aerodynamic force production, flight control and performance limitations. *Journal of Experimental Biology* **219**, 3518–3531.
- Chin, D. D. and Lentink, D.** (2016). Flapping wing aerodynamics: from insects to vertebrates. *J. Exp. Biol.* **219**, 920–932.
- Dickinson, M. H. and Götz, K. G.** (1993). Unsteady aerodynamic performance of model wings at low reynolds numbers. *J. Exp. Biol.* **174**, 45–64.
- Dickinson, M. H., Lehmann, F.-O. and Sane, S. P.** (1999). Wing rotation and the aerodynamic basis of insect flight. *Science* **284**, 1954–1960.
- Ellington, C. P.** (1991). Aerodynamics and the origin of flight. *Adv. Insect Physiol.* **23**, 171–210.
- Ellington, C. P., van den Berg, C., Willmott, A. and Thomas, A. L. R.** (1996). Leading-edge vortices in insect flight. *Nature* **384**, 626–630.

- Garrick, I. E.** (1936). Propulsion of a flapping and oscillating airfoil. *NASA Tech. Rep.* **567**.
- Granlund, K. O., Ol, M. V. and Bernal, L. P.** (2013). Unsteady pitching flat plate. *J. Fluid Mech.* **733**, R5.
- Harbig, R. R., Sheridan, J. and Thompson, M. C.** (2013). Reynolds number and aspect ratio effects on the leading-edge vortex for rotating insect wing planforms. *J. Fluid Mech.* **717**, 166–192.
- Hedrick, T. L., Tobalske, B. W. and Biewener, A. A.** (2002). Estimates of circulation and gait change based on a three-dimensional kinematic analysis of flight in cockatiels (*nymphicus hollandicus*) and ringed turtle-doves (*streptopelia risoria*). *Journal of Experimental Biology* **205**, 1389–1409.
- Lentink, D. and Dickinson, M. H.** (2009). Biofluiddynamic scaling of flapping, spinning, and translating fins and wings. *J. Exp. Biol.* **212**, 2691–2704.
- Liu, B., Hamed, A. M., Jin, Y. and Chamorro, L. P.** (2017). Influence of vortical structure impingement on the oscillation and rotation of flat plates. *J. Fluids and Structures* **70**, 417–427.
- Maxworthy, T.** (1981). The fluid dynamics of insect flight. *Annu. Rev. Fluid Mech.* **13**, 329–350.
- Onoue, K. and Breuer, K.** (2016). Vortex formation and shedding from a cyber-physical pitching plate. *J. Fluid Mech.* **793**, 229–247.
- Onoue, K., Song, A., Strom, B. and Breuer, K.** (2015). Large amplitude flow-induced oscillations and energy harvesting using a cyber-physical pitching plate. *J. Fluids and Structures* **55**, 262–275.

- Parslew, B.** (2014). Predicting power-optimal kinematics of avian wings. *Journal of The Royal Society Interface* **12**.
- Parslew, B. and Crowther, W.** (2010). Simulating avian wingbeat kinematics. *Journal of Biomechanics* pp. 3191–3198.
- Read, T. J. G., Segre, P. S., Middleton, K. M. and Altshuler, D. L.** (2016). Hummingbirds control turning velocity using body orientation and turning radius using asymmetrical wingbeat kinematics. *Journal of The Royal Society Interface* **13**.
- Sane, S. P. and Dickinson, M. H.** (2001). The control of flight force by a flapping wing: lift and drag production. *Journal of Experimental Biology* **204**, 2607–2626.
- Sane, S. P. and Dickinson, M. H.** (2002). The aerodynamic effects of wing rotation and a revised quasi-steady model of flapping flight. *Journal of Experimental Biology* **205**, 1087–1096.
- Stowers, A. K. and Lentink, D.** (2015). Folding in and out: passive morphing in flapping wings. *Bioinspiration & Biomimetics* **10**, 025001.
- Theodorsen, T.** (1935). General theory of aerodynamic instability and the mechanism of flutter. *NASA Tech. Rep.* **496**.
- Tobalske, B. and Dial, K.** (1996). Flight kinematics of black-billed magpies and pigeons over a wide range of speeds. *Journal of Experimental Biology* **199**, 263–280.
- Tobalske, B. W., Hedrick, T. L. and Biewener, A. A.** (2003). Wing kinematics of avian flight across speeds. *Journal of Avian Biology* **34**, 177–184.
- Wagner, H.** (1925). Über die Entstehung des dynamischer Austrieb von Tragflügeln. *ZAMM* **5**, 17–35.
- Wang, Z. J.** (2000). Vortex shedding and frequency selection in flapping flight. *J. Fluid Mech.* **410**, 323–341.

Wong, J. G. and Rival, D. E. (2015). Determining the relative stability of leading-edge vortices on nominally two-dimensional flapping profiles. *J. Fluid Mech.* **766**, 611–625.

Figure Legends

Figure 1

(A) a schematic of the experimental set-up. (B) a definition sketch of the forces and moment acting on a flat plate immersed in a uniform free-stream.

Figure 2

(A)-(D), respectively, illustrate the evolutions of C_L , C_D , C_M and x_{cp}^* as a function of the angle of attack, α .

Figure 3

(A) a schematic of the simulated pigeon model. (B) The predicted wingbeat frequencies of a pigeon during its steady-state forward flight over a range of flight speeds varying from 6 m/s to 20 m/s.

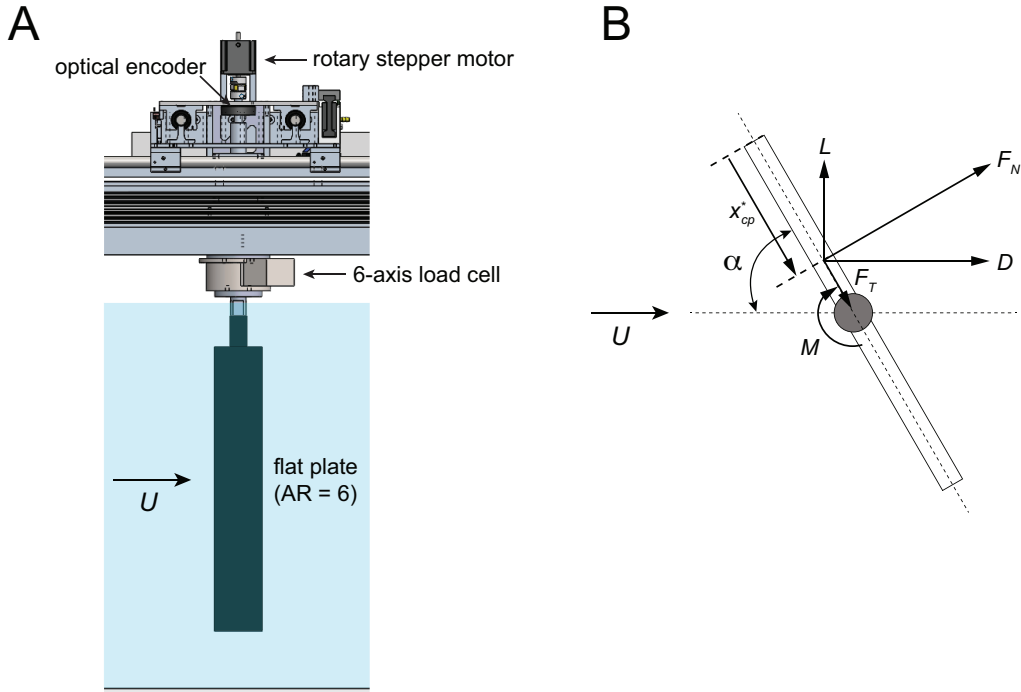


Figure 1: The experimental set-up. (A) schematic of the experimental set-up, illustrating a flat plate ($AR = 6$) mounted on a 6-axis load cell about its mid-chord location. The flat plate is immersed in a uniform flow with a free-stream velocity, U . The present set-up allows for a direct measurement of normal and tangential forces, as well as the pitching moment exerted on a flat plate. The angle of attack, α , is accurately measured and modulated via the optical encoder and the rotary stepper motor using an open-loop command. (B) definition sketch of the forces and moment imparted on a flat plate. Lift and drag are approximated by decomposing the forces (F_N and F_T) into components along the streamwise and transverse directions. The normalized center of pressure, x_{cp}^* , is measured from the leading edge.

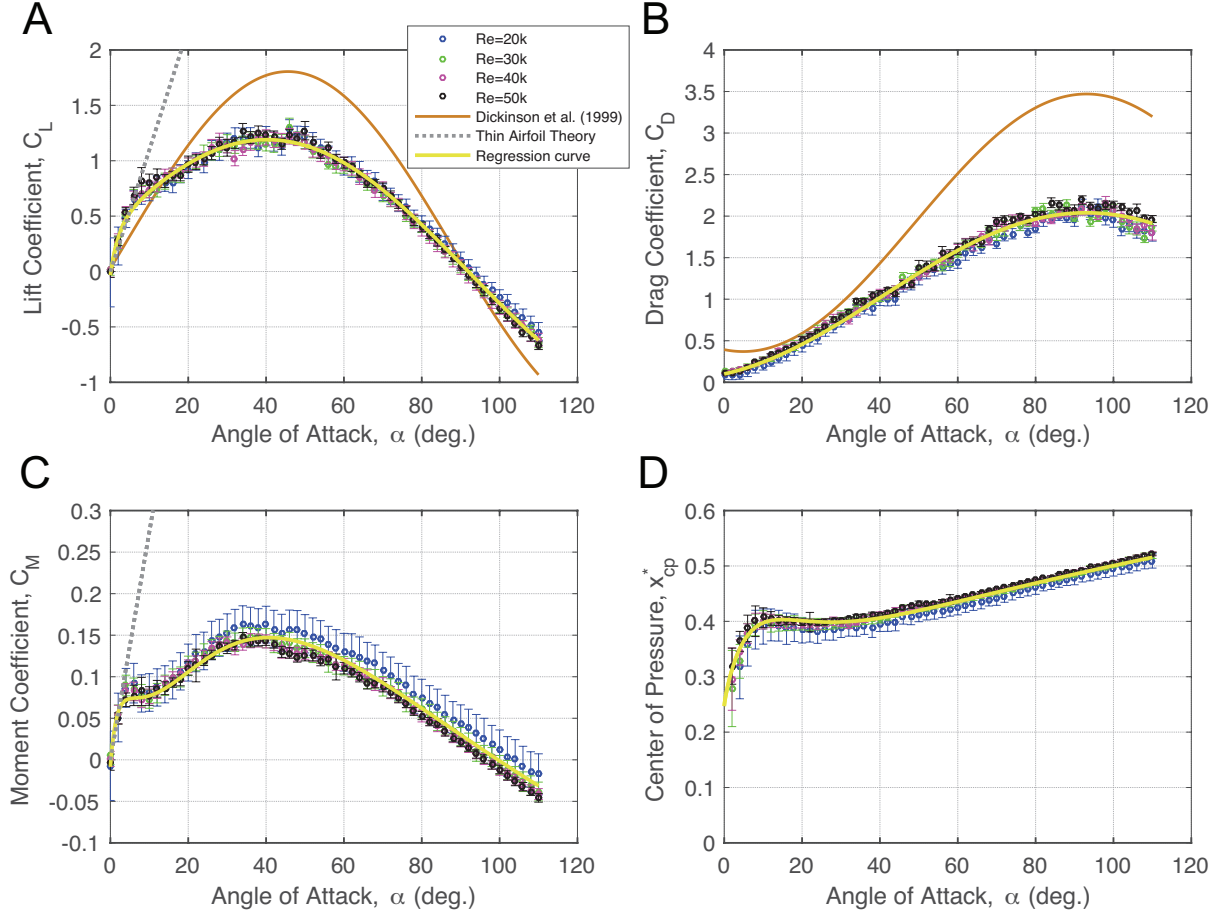


Figure 2: The evolution of normalized lift (A), drag (B), moment (C) and center of pressure (D) as a function of the angle of attack, α , at four distinct Reynolds numbers. Steady-state forces and moment are appropriately normalized by the inertial forcing of the fluid flow. The error bar associated with each data point represents the standard deviation of the time-averaged measurement. Thin airfoil theory predictions of C_L (i.e. $2\pi\alpha$) and C_M (i.e. $\frac{\pi}{2}\alpha$) are plotted with the gray dotted lines in (A) and (C), respectively. The regression curves for C_L , C_D and x_{cp}^* are plotted with the solid yellow curves, where the corresponding equations are provided in Eqns 1 and 2. The regression curve for C_M is deduced analytically using the expressions of C_L , C_D and x_{cp}^* (discussed further in the text).

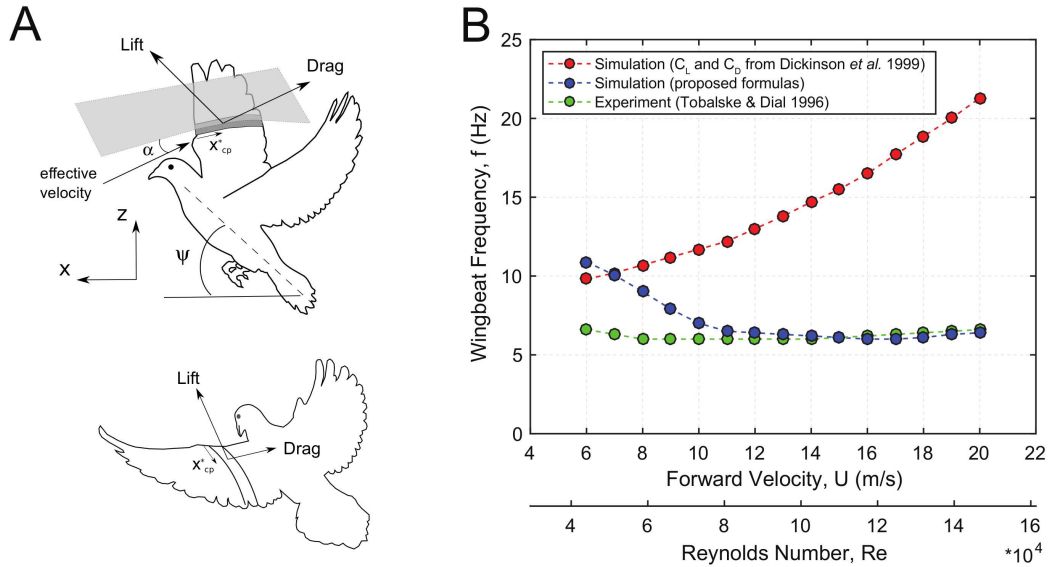


Figure 3: (A) schematic of the simulated pigeon model with two translational degrees of freedom ($x - z$) and one rotational degree of freedom in pitch for the body angle (ψ). In addition to producing flapping and pronation/supination motions, the model can modulate its wingspan during the wingbeat cycles. (B) predicted wingbeat frequency of the pigeon during its steady forward-flight over a range of flight velocities varying from 6 m/s to 20 m/s. Red dots represent the wingbeat frequencies evaluated using the quasi-steady aerodynamic formulations of Dickinson *et al.* (1999). Blue dots designate the predicted wingbeat frequencies using the proposed aerodynamic formulas, revealing an improved agreement with the previously-reported experimental data on pigeons (green dots) by Tobalske and Dial (1996), in particular for high forward velocities (i.e. $U > 10$ m/s).

This figure "JEB_Instruction.png" is available in "png" format from:

<http://arxiv.org/ps/2302.09602v1>